NASA TN D-1919

TECHNICAL NOTE

D-1919

A CONTRIBUTION TO THE THEORY OF PRESSURE STABILIZED STRUCTURES

By

A. C. Kyser

Prepared under Contract NASr-8 by
ASTRO RESEARCH CORPORATION
Santa Barbara, California

for

NATIONAL AERONAUTICS AND SPACE ADMINISTRATION

WASHINGTON May 1963

TABLE OF CONTENTS

LIST OF ILLUSTRATIONS

LIST OF SYMBOLS

a	compression-induced spread of centers of curvature
b	shear-induced spread of centers of curvature
e	shear deflection
F	externally applied lateral compression force per unit length of cylinder
h	height of cross section
M	externally applied rolling moment per unit length of cylinder
p	internal pressure
Q	externally applied shear force per unit length of cylinder
s	length of flexible membrane between flats
T	circumferential-direction membrane tension per unit length of cylinder
w	width of flat
α	angle of membrane arc included between reference plane and lower flat
β	angle of membrane arc included between reference plane and upper flat
σ	central half-angle included by membrane arc
γ	angular deflection due to shear load
θ	angular deflection between flats due to rolling moment
ρ	radius of curvature of membrane

NATIONAL AERONAUTICS AND SPACE ADMINISTRATION

TECHNICAL NOTE D-1919

A CONTRIBUTION TO THE THEORY OF PRESSURE STABILIZED STRUCTURES

By

A. C. Kyser

SUMMARY

A large-deformation analysis is presented for an element of a flexible inflatable plate consisting of an array of contiguous tubes. The element is represented by a transversely-loaded pressurized cylindrical chamber of indefinite length having two flat sides connected by flexible but inextensible membranes. The behavior of the cylindrical element is described for the complete range of deformation for the case of lateral compression, shear, or rolling loads, and a method is described for obtaining a graphical solution for the shape of the cross section under any given combination of loads. It was found that under certain conditions large compressive deformations give rise to geometrical instabilities, or conditions of negative spring rate.

I. INTRODUCTION

The load-vs-deformation behavior of inflatable structures is a subject that has received considerable attention in recent years. This subject has special importance in the design of light-weight deployable structures for space applications. In Reference 1 this general problem is discussed with special emphasis given to a theory for deflections of a type of inflatable plate known as "Airmat," which has been developed by the Goodyear Aircraft Corporation. The Airmat construction consists of a flexible sandwich having flexible skins connected together by a core of closely-spaced "drop cords." The sandwich-core chamber is pressurized to produce the desired plate stiffness. The problems of static deflection and of vibration of this type of structure are treated in References 2 and 3.

In certain applications for expandable pressure-stabilized plates, the presence of closely-spaced drop cords may be undesirable because of requirements for internal space, foldability, or minimum weight. For such applications, the requirements may dictate the use of an alternate construction for inflatable plates. One possible configuration consists of an array of parallel contiguous cylindrical tubes such as that shown in Figure 1. This type of plate structure was discussed briefly in Reference 1. Such a structure will be anisotropic in the sense that its load-vs-deformation characteristics (up to the buckling load) along the direction of the cylinders will depend primarily on the properties of the materials of which the construction is made, whereas the resistance to deformation across the tubes will depend primarily on the pressure and the tube geometry.

The subject of the present paper is a fundamental investigation of the basic mechanism by which an inflatable structure of this type transmits load across the array of tubes. The analysis has been restricted to a single idealized element of the array, consisting of an indefinitely long cylindrical chamber made from completely flexible but inextensible material.

The deformations of a structure of this type take place without changing the load-carrying ability of the materials which make up the structure. Thus, the usable range of deformations is not limited to small deflections in the usual sense. Because of the importance associated with developing an understanding of the non-linear large-deformation behavior of this type of inflatable structure, the analysis was made rigorously, without resort to the limiting assumptions of small deflection theory. The results which are presented are, therefore, valid for the entire range of possible deformations.

II. ANALYSIS

A. Description of the Problem

The inflatable structural element under consideration here is a pressurized cylinder of indefinite length having a cross section as shown in Figure 2. The cylinder is constructed with two flat, rigid walls simulating the webs and the symmetry conditions imposed by the adjoining elements, connected together at their edges by flexible membranes representing the cover of the plate-like structure. Under internal pressure, the cross section assumes a preferred shape and the cylinder exhibits stiffness against loads which would change the relative positions of the webs, or flats.

Deformations considered here are those resulting from loads (either normal or shear forces or rolling moments) applied to the webs in directions parallel to the plane of the cross section. These loads represent the internal shear forces, lateral compression, and bending moments of the plate-like structure. In all cases the loads are taken to be uniformly distributed along the length of the cylinder, so that there is no load transferred between sections of the cylinder. The problem can therefore be treated with a two-dimensional analysis. The matter of end closures for the cylinder is not considered.

The assumption has been made that the internal pressure is both uniform throughout the cylinder, and invariant with changes in geometry of the cross section. It has also been assumed that the flats of the cylinder are of fixed widths and that the membranes are inextensible, with no stiffness in bending.

For the sake of simplicity, the discussion has been restricted to those cases for which the flats are equal in width and the membranes equal in arc length. The arcs formed by the membranes in cross section are circular, since the radius of curvature is determined by the pressure and tension, which are uniform. In the initial geometry, shown in Figure 2, these circular arcs have a common center; thus, the undeformed cross section is that of a right circular cylinder with flats on opposite sides.

It will be seen that any deformation under load must come about as a result of a reorienting of the various inextensible components, rather than as a result of elastic behavior of the components themselves. In this regard, this structural element behaves in a manner that is more nearly representative of the kinematic mechanism than of the classical "structure."

B. Method of Analysis

To establish the cross-sectional shape of the cylinder under any given loading condition, a set of equations of equilibrium can be written for the

forces acting on the flats. These forces include the applied load and the pressure load, as well as the undetermined tension loads in the membranes, which act at undetermined angles to the flats. The equations of equilibrium, together with the geometrical requirements, form a set of simultaneous, transcendental, algebraic equations which, in principle, can be solved to obtain the parameters of the cross-section geometry.

In the simpler cases these equations can be reduced algebraically to useful form, which generally involves a geometrical parameter such as the central angle of the membrane arc. In the more complex cases no such reduction has been found, and the application of the equations is limited to numerical evaluation for specific cases.

In all cases, however, it is a simple matter to establish the relative positions of the centers of curvature of the two arcs, provided the loads on either flat are known. Once the centers of curvature are established, it is possible to establish loci of position for the four corners of the cross section on which these corners must lie. The desired solution for the cross section shape can be obtained easily by graphical iteration on the plots of the loci.

The details of the analysis for the various types of deformation are presented in the Appendix. A summary of the results of the analysis is given in the following section.

C. Load-vs-Deformation Behavior

(1) Deformation Under Lateral Compression Loads: The cross-section geometry for deformation under lateral compression load is shown in Figure 3. The nature of this deformation is such that the curvature of the membranes increases and the membrane tension decreases with increasing load. The centers of curvature are spread apart in the direction normal to the load direction by an amount which is proportional to the load. As in all cases considered in this paper, the arc length of the membrane remains invariant. It is this condition which establishes the height of the cross section for any load.

A set of curves of normalized compression load-vs-deformation for several ratios of arc length to flat width are shown in Figure 4. The normalized spring rate is shown by the curve set in Figure 5, for which the abscissa is the central half-angle of the membrane arc. For deformations for which this angle tends to become larger than 90°, two cases are of interest. If the cylinder is an element of a multicell structure, there may be a restriction on the deformed cross section such that no portion of the membrane can extend outside the region between the planes of the flats. In this case the membranes of adjacent chambers will converge to produce an apparent widening of the common flat, along with an accompanying shortening of the effective arc lengths of the membranes. This mode of deformation is

such that the central half-angle becomes fixed at 90°. Since the compression spring rate is dependent only on the pressure and the central angle, the cylinder then behaves like a linear spring (under the assumption of constant pressure). This effect is shown by the dotted portion of the load-vs-deformation curves of Figure 4.

If there are no external restrictions on the shape of the cross section, the central angle will continue to increase with increasing load, so that the membrane arc is greater than a semicircle. As the deformation is increased, the spring rate continues to decrease until a point is reached at which the spring rate curve goes through zero, which is to say that the ability of the cylinder to support compression loads is at a maximum, and further deformation will occur without increase of load. The zero-spring-rate geometry is diagrammed in Figure 6. The value of the central half-angle for this condition is 160°. This phenomenon reflects a "geometrical instability," or a condition in which the instability of the structure results from its geometrical arrangement alone, rather from a combination of geometry and material properties.

(2) Deformation Under Shear Loads: The conditions necessary for producing a pure shear deformation of the cylinder are shown in Figure 7. If the shear loads are applied in the planes of the flats, as shown, an externally-applied righting moment is necessary for equilibrium. This righting moment has the effect of shifting the shearing-load planes of action to the mid-plane of the cylinder. The effect of the shearing load on the geometry of the cross section is to cause the centers of curvature to be shifted apart in a direction that is perpendicular to the load by an amount that is proportional to the load. The membrane tension increases with increasing shear load. It can be shown that the initial shear behavior of the cylinder is the same as that of a rectangular shear pad having the height of the cylinder, the width of the flat, and a shear modulus of elasticity equal to the internal pressure.

(3) Deformation Under Rolling-Moment Load: The deformation of the cross section under a lateral rolling moment applied to the flats is shown in Figure 8. In this case the centers of curvature remain coincident, but are shifted away from the original position with respect to the webs. The amount of this shift is such that the difference between the squares of the radii is proportional to the applied moment.

An analytical expression has not been found for this case to allow the cross-section parameters to be computed explicitly as a function of load. A graphical solution has been worked out, however, for obtaining a load-vs-deformation curve for any given initial geometry. The method, as shown in Figure 9, consists of fixing the position of the center of curvature and the direction of the plane of symmetry, and establishing loci of position for the corners of the cross section. These loci are mirror-image hyperbolic spirals about the center of curvature. Once the loci are established, the

rolling moment for any given roll position of the plate can be determined graphically by measuring the radii of curvature.

(4) Deformation Under Combined Loads: The effect on the cross section of loads having compression, shear, and rolling components is such that the total shift of the centers of curvature is the same as that which would be computed by adding the shifts caused by the three components taken individually. Thus, the pattern for the centers of curvature can be determined directly from the loads. Figure 10 shows a deformation of this type.

To determine the cross-section shape analytically requires, in the general case, solution of five simultaneous transcendental equations with five unknowns. As in the case of the rolling-moment load, however, the general problem can be solved by a graphical approach involving loci of position for the corners of the cross section about the "fixed" pattern of centers. In this case the solution involves a graphical iteration around the diagram, as shown in Figure 11. The procedure is described in detail in the Appendix.

The special case of combined shear and compression is of interest because of its simplicity. It can be shown that the effect of a fixed compression load on the shearing behavior of the cylinder is the same as the effect of a decrease in the width of the flat by an amount equal to the spread of the centers due to the compression load; in other words, the shear behavior is determined by the membrane geometry independently of the width of the flat. If the compression-induced spread of the centers is equal to the width of the flat, the shear stiffness is zero, and for greater compression loads the shear spring rate of the cylinder becomes negative. This condition reflects, as in the case of a lateral normal load discussed above, a form of geometrical instability, i. e., one which is independent of the properties of materials used in the construction of the cylinder.

III. EXPERIMENT

In order to verify the theoretical work and to observe the large-deformation behavior of a physical model, a series of experiments were undertaken. In these experiments, a partially flexible cylinder was pressurized with water at a constant pressure level and loaded with lead weights. Deformations were measured with dial-indicator gages.

The model is shown in Figure 12 and the experimental setup in Figure 13. The cylinder was fabricated by winding dry fiberglass roving over a mandrel on which were mounted two 3/16-inch thick aluminum plates, one on each side. After completion of the winding, the fibers were bonded between these inner plates and a set of outer plates. The fiberglass was left unbonded in the "membrane" region to retain minimum bending stiffness. A pressure-tight bladder was fabricated by making a tube from a sheet of natural rubber about .020 inch thick and binding the ends to rubber stoppers. The end-cap load was accounted for by supporting the bladder with an oversized knit bag which was stretched longitudinally to minimize circumferential stiffness.

To eliminate the effects of the end restraints, the upper plates were segmented three inches from each end of the cylinder. The separate end pieces were adjustable to allow aligning with the center section for each new load, and held in position with bolts from the base plate, as shown in the photograph.

The cylinder was pressurized hydrostatically from a standpipe about 14 ft. high. An overflow near the upper end of the standpipe allowed the pressure to be maintained at a constant level. Volume-change measurements were made by collecting and weighing the water discharged at the overflow. The internal pressure for these tests was 6.2 psi.

Compression loads were applied in the form of weights placed on a stiff beam supported by the upper plate, as shown in Figure 13. It was found that seemingly minor deviations from uniformity in the winding resulted in a somewhat erratic initial behavior under compression loads. By applying a sufficiently large tare load, however, it was found that the behavior of the cylinder for higher loads was reasonably close to the theoretical predictions. The deflection was measured with a dial-indicator gage at three points on the beam.

The results of the compression load test are shown in Figures 14 and 15. On these plots, the initial tare-load values have been set up to lie on the theoretical curve, with the other values in correct position relative to the tare values.

In the shear tests, the cylinder was loaded through a bridle such

that the load was applied in the horizontal mid-plane between the upper and lower plates. An upward force was used to counteract the weight of the loading apparatus on the upper plate so that a pure shear deformation was obtained. The shear offset e was measured with dial gages near the ends of the cylinder. Figure 16 shows the results of the shear test.

The roll test was set up with the cylinder loaded by a force couple through a torsion bar clamped to the top plate of the cylinder. The roll angle θ was measured as deflection of two points on a rod attached to the torsion bar. The results are shown in Figure 17. The theoretical curve for this figure was determined by graphical construction.

One case of deformation under a combined load was included in the test program. For this case, the cylinder was loaded simultaneously with compression, shear, and rolling loads, and measurements were made of the deformation. A theoretical prediction of the deformation was obtained using the graphical iteration method described in the Appendix. A comparison of the measured and theoretically-determined deformed cross sections is shown in Figure 18.

Astro Research Corporation
Santa Barbara, California
September 24, 1962

APPENDIX

A. Initial Geometry

The structural element under consideration is a pressurized cylinder of indefinite length having two flat rigid sides which are connected together at their edges by flexible membranes, as shown in Figure 2. The widths of the flat sides are taken to be equal, as are the arc lengths of the membranes. Loads are applied to the cylinder through the flats, in the form of distributed forces and rolling moments tending to distort the cross section. It is assumed that all loads act in directions parallel to the plane of the cross section, and that all sections along the length of the cylinder are loaded equally so that there is no load transferred between sections. It is further assumed that the flats are rigid and that the membranes are inextensible, but perfectly flexible.

To establish the shape of the unloaded cylinder we can write the conditions for equilibrium of the lower plate as shown in Figure 2. It will be seen that for zero load the forces on a unit length of the cylinder must be such that

$$2T_o \cos\alpha_o = pw \quad , \tag{A-1}$$

where p is the internal pressure, w and α are as shown in Figure 1, and the subscript o stands for the no-load condition. The tension T_o is the circumferential-direction tension force carried by the membrane per unit length of the cylinder. With elementary cylinder theory it can be shown that

$$T_o = p\rho_o \quad . \tag{A-2}$$

Substitution of equation (A-2) into equation (A-1) gives

$$2\rho_o \cos\alpha_o = w \quad , \tag{A-3}$$

which is to say that the centers of curvature of the flexible sides coincide; i.e., equation (A-3) establishes "vertical" alignment of the centers, while "horizontal" alignment is required by symmetry. The unloaded cylinder therefore has the shape of a circular cylinder with flats on opposite sides. To establish the distance h_o between the flats, given the arc length s and the width w, note that

$$\frac{s}{2} = \rho_o \alpha_o \quad . \tag{A-4}$$

Thus, from equation (A-3),

$$\frac{s}{\alpha_o} \cos\alpha_o = w \quad . \tag{A-5}$$

Further,

$$h_o = 2\rho_o \sin\alpha_o = \frac{s}{\alpha_o} \sin\alpha_o \quad . \tag{A-6}$$

Dividing equation (A-5) by equation (A-3) gives

$$\frac{h_o}{w} = \tan\alpha_o \quad , \tag{A-7}$$

and squaring and adding gives

$$\left(\frac{s}{\alpha_o}\right)^2 = w^2 + h_o^2 \quad . \tag{A-8}$$

Solving equations (A-7) and (A-8) to eliminate α_o , it is seen that the condition for h_o is

$$\frac{s^2}{w^2 + h_o^2} = \left[\arctan \frac{h_o}{w}\right]^2 \quad . \tag{A-9}$$

This equation is readily solved numerically by iteration or by any other method for finding the roots of a transcendental equation. Another approach is to solve equation (A-5) iteratively for the parameter α_o , which can then be used in equation (A-6) to give h_o .

B. Deformation Under Compression Loads

If the cylinder is loaded symmetrically with a compression force, the plates will be displaced toward the center plane. Since the arc lengths are fixed, the curvature of the membranes must increase. The cross section will, therefore, assume a shape like that shown in Figure 3. The new equilibrium requirements are given by

$$2T \cos\alpha + F = pw$$

or

$$2\rho \cos\alpha = w - \frac{F}{p} \quad . \tag{B-1}$$

The geometry of the cross section is such that

$$2\rho \cos\alpha = w - a \quad . \tag{B-2}$$

Therefore,

$$a = \frac{F}{p} \quad ; \tag{B-3}$$

that is, the spacing between the centers of curvature is directly proportional to the compressive load.

Given the plate width, the arc length, and the load, the angle α can be determined readily. Noting that $2\rho\alpha = s$, it is convenient to rewrite equation (B-2) as

$$\frac{\cos\alpha}{\alpha} = \frac{w - a}{s} \tag{B-4}$$

To find the deformation-vs-load characteristic (i. e., to find h as a function of F) , the following geometrical relations can be used:

$$h = 2\rho \sin\alpha = \frac{s}{\alpha} \sin\alpha \tag{B-5}$$

Combining equation (B-5) with equation (B-2) to eliminate α gives

$$\frac{s^2}{h^2 + (w - a)^2} = \left[\arctan\left(\frac{h}{w - a}\right)\right]^2 \tag{B-6}$$

The spring rate with which the cylinder resists incremental deformation by compressive loads is $\left(-\frac{dF}{dh}\right)$. To compute this it is convenient to perform the differentiation with respect to the parameter α :

$$\left(-\frac{dF}{dh}\right) = -\frac{dF/d\alpha}{dh/d\alpha} \tag{B-7}$$

From equations (B-3) and (B-4)

$$F = p\left[w - \frac{s}{\alpha}\cos\alpha\right] ,$$

which gives

$$\frac{dF}{d\alpha} = ps\left[\frac{\alpha \sin\alpha + \cos\alpha}{\alpha^2}\right] . \tag{B-8}$$

Also, from equation (B-5)

$$\frac{dh}{d\alpha} = s\left[\frac{\alpha \cos\alpha - \sin\alpha}{\alpha^2}\right] . \tag{B-9}$$

Thus

$$\left(-\frac{dF}{dh}\right) = p\left[\frac{\cos\alpha + \alpha\sin\alpha}{\sin\alpha - \alpha\cos\alpha}\right] \qquad (B\text{-}10)$$

This function can be expressed in terms of h and F by the use of equations (B-3), (B-4), and (B-5):

$$\left(-\frac{dF}{dh}\right) = p\left[\frac{2\rho(w-a) + sh}{2\rho h - s(w-a)}\right] \qquad (B\text{-}11)$$

where

$$2\rho = \sqrt{h^2 + (w-a)^2}$$

The spring rate of the cylinder against deformation from its initial, no-load geometry can be obtained by setting $a = 0$ in equation (B-11):

$$\left(-\frac{dF}{dh}\right)_o = p\left[\frac{w\sqrt{h_o^2 + w^2} + sh_o}{h\sqrt{h_o^2 + w^2} - sw}\right] . \qquad (B\text{-}12)$$

The special case $w = 0$ represents the condition for a concentrated line load on a flexible cylinder. For this case, of course, $\alpha_o = \frac{\pi}{2}$, and $h_o = 2\rho_o = \frac{s}{\pi/2}$. The initial spring rate is, from equation (B-12), for this case:

$$\left(-\frac{dF}{dh}\right)_o = p\left[\frac{s}{h}\right] = p\left[\frac{\pi}{2}\right] \qquad (B\text{-}13)$$

Note the lack of dependence on diameter.

Equation (B-10) shows that the spring rate in general is determined only by the pressure and the angle α. An interesting result of this can be seen from a consideration of a flexible cylinder compressed between two wide parallel plates, representing the situation in a multiple-chambered plate-like structure compressed laterally beyond the point where two membranes joining at a web form a finite angle. It is apparent that $\alpha = \frac{\pi}{2}$ for any compressed position of such a cylinder. Thus, from equation (B-10)

$$\left(-\frac{dF}{dh}\right) = p\left[\frac{\pi}{2}\right]$$

Thus, the compressed cylinder (with constant internal pressure) behaves like a linear spring.

A geometrical interpretation of equation (B-10) is given in Figure 19 which shows the involute of a unit circle. Here the angle α is the angle swept by the tangent to the generating radius r, while φ is the central angle swept out by the involute curve about the center of the unit circle. The Cartesian coordinates of the involute are

$$y = \sin\alpha - \alpha\cos\alpha$$

$$x = \cos\alpha + \alpha\sin\alpha$$

Note that

$$\cot\varphi = \frac{x}{y} = \frac{\cos\alpha + \alpha\sin\alpha}{\sin\alpha - \alpha\cos\alpha} \tag{B-14}$$

Thus the spring rate is

$$\left(-\frac{dF}{dh}\right) = p\cot\varphi \tag{B-15}$$

This relation may be expressed in terms of compliance:

$$\left(-\frac{dh}{dF}\right) = \frac{1}{p}\tan\varphi \tag{B-16}$$

Note that the compliance, $\tan\varphi$, is numerically equal to the y value of the intersection of the line $\overline{OP}$ and the line (shown dashed) $x = 1$. It is readily seen that the compliance can change by a very large factor. Indeed, at the angle at which the involute curve crosses the y axis the compliance becomes infinite (i.e., the spring rate is zero) and thereafter is negative. This occurs at

$$-\cot\alpha = \alpha = 2.80 = 160^\circ$$

The geometry for this condition is shown in Figure 6.

A geometrical interpretation of the stiffness relation is shown in Figure 20. The origin O for this diagram is the center of curvature of the flexible side of the cylinder, while the curve is the locus of the "corner" of the cross section as α changes, with the center of curvature remaining stationary and the plate moving parallel to its original position. The polar coordinates (ρ, α) of this locus must satisfy the equation

$$\rho\alpha = \frac{s}{2}$$

This equation describes a hyperbolic spiral. Its Cartesian coordinates are

$$\left.\begin{aligned} y &= \rho \sin\alpha = \frac{h}{2} \\ x &= \rho \cos\alpha = \frac{w-a}{2} \end{aligned}\right\} \qquad \text{(B-17)}$$

Now consider in the light of this diagram the behavior of the cylinder under a compression load. If an incremental load ΔF is added to the load F, the centers of curvature of the sides will move outward from the centerline of the cylinder a distance of $\frac{1}{2}\Delta a = \frac{1}{2}\frac{\Delta F}{p}$. Referred to the diagram of Figure 20, this distance is a horizontal displacement of the corner by an amount $\frac{1}{2}\frac{\Delta F}{p}$ in the direction of the origin. Accompanying this horizontal displacement is a vertical displacement of $-\frac{1}{2}\Delta h$. Thus, the change in height per unit of change in load (i. e., the compliance of the cylinder) is represented by the slope of the spiral:

$$\frac{\Delta y}{\Delta x} = \frac{-\Delta h/2}{\Delta F/2p} = p\left(-\frac{\Delta h}{\Delta F}\right)$$

or (B-18)

$$-\frac{dh}{dF} = \frac{1}{p}\frac{dy}{dx} = \frac{1}{p}\tan\varphi$$

where φ is the slope angle of the spiral. It can be readily verified that the slope of the spiral gives the same function $\varphi(\alpha)$ as the central angle of the involute of the unit circle.

Figure 4 shows a set of curves for the normalized lateral compression load-vs-deflection for several values of the geometrical parameter s/w and for deformations either unrestrained or limited by adjoining elements. The spring rate for any particular condition is the slope of the curve at the point in question. The $\alpha = 90^\circ$ contour where the deformation characteristics branch due to restraints coincides with the line $\frac{F}{pw} = 1$.

Figure 5 is a plot of normalized spring rate vs the angle α. F has been normalized by the factor pw and h has been normalized by h_o. The initial-condition contour is also shown. For these normalizing references, the initial spring rate has a minimum near $\alpha_o = 60^\circ$.

C. Deformation Under Shearing Loads

The deformed shape of a cylinder subjected to a shearing load is shown

in Figure 7. It can be seen from this diagram that, for reasons of symmetry,

$$\left.\begin{aligned} \rho_1 &= \rho_2 = \rho \\ \alpha_1 &= \beta_2 \; ; \; \beta_1 = \alpha_2 \\ \sigma &= \frac{\alpha_1 + \beta_1}{2} = \frac{\alpha_2 + \beta_2}{2} \\ \gamma &= \frac{\beta_1 - \alpha_1}{2} = \frac{\alpha_2 - \beta_2}{2} \end{aligned}\right\} \qquad (C\text{-}1)$$

An externally-applied righting moment is necessary for roll equilibrium of the cylinder. To maintain anti-symmetry, let the moments applied to the upper and lower plates be equal. Thus,

$$M = \frac{Qh}{2} \qquad (C\text{-}2)$$

This moment has the value necessary to shift the shearing loads to the mid-plane of the cylinder.

The condition for equilibrium of vertical forces on the lower plate is that

$$T_1 \cos\alpha_1 + T_2 \cos\alpha_2 = pw$$

Recalling that

$$T = p\rho \; ,$$

we may write this as

$$\rho \cos\alpha_1 + \rho \cos\alpha_2 = w \qquad (C\text{-}3)$$

Thus, the horizontal displacement between the centers of curvature, corresponding to the distance a in the compression case, is zero.

Equilibrium of the lateral forces on the lower plate demands that

$$T_1 \sin\alpha_1 + Q = T_2 \sin\alpha_2$$

which is to say that

$$\rho\sin\alpha_2 - \rho \sin\alpha_1 = \frac{Q}{p} \qquad (C\text{-}4)$$

By comparing this expression with the requirements of the geometry of the cross section, it can be seen that

$$b = \frac{Q}{p} ; \qquad (C-5)$$

i. e., the vertical displacement between the centers is proportional to the shear load.

Adding the moments which tend to rotate the lower plate about its right-hand corner, we see that

$$T_1 \cos\alpha_1 \cdot w = \frac{pw^2}{2} + M$$

Substitution of equations (2) and (5) gives

$$\rho \cos\alpha_1 = \frac{w}{2} + \frac{bh}{2w} \qquad (C-6)$$

Similarly

$$\rho \cos\alpha_2 = \frac{w}{2} - \frac{bh}{2w} \qquad (C-7)$$

Another basic condition for the cross section is given by the geometry:

$$\rho \sin\alpha_1 + \rho \sin\beta_1 = h \qquad (C-8)$$

Finally, the condition for fixed arc length yields:

$$s = \rho(\alpha_1 + \beta_1) = \rho(\alpha_2 + \beta_2) = 2\rho\sigma \qquad (C-9)$$

This condition is more conveniently handled in terms of σ . Substituting σ and γ for α and β in equations (C-3), (C-4), (C-6), (C-8) yields the following equations for the cross section:

$$\frac{s}{\sigma} \cos\sigma \cos\gamma = w \qquad (C-10)$$

$$\frac{s}{\sigma} \cos\sigma \sin\gamma = b \qquad (C-11)$$

$$\frac{s}{\sigma} \sin\sigma \cos\gamma = h \qquad (C-12)$$

$$\frac{s}{\sigma} \sin\sigma \sin\gamma = \frac{bh}{w} = e \qquad (C-13)$$

The fourth relation is redundant but is included for convenience. Here, e is the shear offset.

From these relations it can be seen that

$$\tan\sigma = \frac{h}{w} = \frac{e}{b} \qquad \text{(C-14)}$$

$$\tan\gamma = \frac{b}{w} = \frac{e}{h} \qquad \text{(C-15)}$$

If equations (C-10) through (C-13) are squared and then added the result is

$$\left(\frac{s}{\sigma}\right)^2 = w^2 + b^2 + h^2 + e^2 \qquad \text{(C-16)}$$

Equations (C-14) and (C-16) can be combined to eliminate σ , in order to obtain a relation for h :

$$\frac{s^2}{w^2 + b^2 + h^2 + e^2} = \left[\arctan\frac{h}{w}\right]^2 \qquad \text{(C-17)}$$

If it is desired to find h it is possible to solve equation (C-17) numerically. An alternate and possibly more expedient approach is to solve first for the angle σ . A convenient expression for σ can be obtained by squaring and adding equations (C-10) and (C-11):

$$\frac{\cos\sigma}{\sigma} = \frac{\sqrt{w^2 + b^2}}{s} \qquad \text{(C-18)}$$

This relation is readily solved numerically by iteration.

The shear spring rate can be determined from equation (C-15):

$$Q = pw\tan\gamma$$

Thus

$$\frac{dQ}{d\gamma} = \frac{pw}{\cos^2\gamma} \qquad \text{(C-19)}$$

Initially, $\cos\gamma = \cos\gamma_o = 1$. The initial shear spring rate is therefore

$$\left(\frac{dQ}{d\gamma}\right)_o = pw \qquad \text{(C-20)}$$

D. Deformation Under Rolling Loads

Consider now the deformation of the cylinder under a rolling moment

applied to the plates. It can be seen that in the absence of a net shearing or compressive force the centers of curvature for the membranes will coincide. The deformed cylinder will therefore have a cross-section shape of the nature of that shown in Figure 8. The condition for equilibrium of vertical forces on the lower plate is

$$\frac{s}{2\sigma_2}\cos\sigma_2 + \frac{s}{2\sigma_1}\cos\sigma_1 = w\cos\frac{\theta}{2} \tag{D-1}$$

Similarly, the horizontal equilibrium is

$$\frac{s}{2\sigma_2}\sin\sigma_2 - \frac{s}{2\sigma_1}\sin\sigma_1 = w\sin\frac{\theta}{2} \tag{D-2}$$

These relations can be squared and added together to eliminate θ :

$$\left(\frac{s}{2\sigma_1}\right)^2 + \left(\frac{s}{2\sigma_2}\right)^2 + 2\left(\frac{s}{2\sigma_1}\right)\left(\frac{s}{2\sigma_2}\right)\cos\left(\sigma_1 + \sigma_2\right) = w^2 \tag{D-3}$$

Note that this is the law of cosines for the triangle defined by the center of curvature and the plate.

A second equation relating σ_1 and σ_2 can be obtained by taking moments about a section through the horizontal centerplane:

$$\left(T_2 - T_1\right)\left(\frac{\rho_1 + \rho_2}{2}\right) = M ,$$

or

$$\left(\frac{s}{2\sigma_2}\right)^2 - \left(\frac{s}{2\sigma_1}\right)^2 = \frac{2M}{p} \tag{D-4}$$

Equations (D-3) and (D-4) can be solved simultaneously for σ_1 , and σ_2 as functions of M . One scheme for accomplishing this numerically is to iterate with the system

$$\left.\begin{aligned}\left(\frac{s}{2\sigma_2}\right)^2 &= \frac{2M}{p} + \left(\frac{s}{2\sigma_1}\right)^2 \\ \left(\frac{s}{2\sigma_1}\right)^2 &= w^2 - \left\{\left(\frac{s}{2\sigma_2}\right)^2 + 2\left(\frac{s}{2\sigma_1}\right)\left(\frac{s}{2\sigma_2}\right)\cos\left(\sigma_2 + \sigma_1\right)\right\}\end{aligned}\right\} \tag{D-5}$$

Here a value is assumed for σ_1 , and a value for σ_2 is computed from the first equation. These two values are then used on the right side of the second equation to compute an improved value for σ_1 , which is then used in the first equation to recompute σ_2 , etc. Once the parameters σ_1 and σ_2 are calculated, the remaining dimensions of the cross section can be determined immediately.

A graphical method of solving this problem is shown in Figure 9. In this diagram the curves represent the loci of the two corners of the lower plate for a succession of deformed cross-section shapes, all plotted on the diagram with the centers of curvature at the origin and the horizontal centerlines coincident. The polar coordinates of any point on the locus are (ρ, σ) . Since all points along the curves have in common the arc length $\frac{s}{2}$ from the centerline, the curves must satisfy the equation

$$\rho\sigma = \frac{s}{2}$$

This is the equation of a hyperbolic spiral, as discussed in conjunction with Figure 20.

The two loci of position for the corners are therefore mirror-image spirals about the fixed center of curvature. Once these spirals have been established for any given initial geometry, a point on the curve M vs θ can be determined by connecting the two spirals with a line of length w . The angle θ can then be measured directly, and the moment can be computed from equation (D-4); i. e.,

$$\rho_2^2 - \rho_1^2 = \frac{2M}{p} \qquad \text{(D-6)}$$

It is also of interest to note that if the position of the lower plate is retained as the coordinate basis the lateral shift of the center of curvature is proportional to the moment. This can be established by taking moments about the right-hand corner of the lower plate:

$$T_1 \cos\alpha_1 \cdot w = pw \cdot \frac{w}{2} - M$$

or

$$\rho \cos\alpha_1 = \frac{w}{2} - \frac{M}{pw} \qquad \text{(D-7)}$$

Thus the lateral shift of the center is $\frac{M}{pw}$.

An expression for the initial stiffness may be derived using the model

of Figure 9. It can be seen that for small displacements from the initial (symmetrical) geometry, a slight shift of the plate will produce equal changes in the x coordinates of the corners and equal but opposite changes in the y coordinates. As a result of such a shift of an amount Δx, the plate will be tilted by a small angle $\frac{\theta}{2}$, where

$$\frac{\theta}{2} = \frac{\Delta y_2 - \Delta y_1}{w} = \frac{2\Delta y}{w}$$

But

$$\Delta y = \frac{dy}{dx}\Delta x \qquad \text{(D-8)}$$

Thus

$$\frac{\theta}{2} = \frac{2\Delta x}{w}\frac{dy}{dx}$$

From equation (D-6) it can be seen that

$$\frac{2M}{p} = \rho_2^2 - \rho_1^2 = (\rho_2 + \rho_1)(\rho_2 - \rho_1) = 2\rho_o \cdot 2\Delta\rho \qquad \text{(D-9)}$$

where ρ_o is the initial radius of curvature and $\Delta\rho$ is the change in ρ resulting from Δx. It can also be seen from the diagram that

$$\Delta\rho = \Delta x\sqrt{1 + \left(\frac{dy}{dx}\right)_o^2}\cos(\sigma_o - \varphi_o) \qquad \text{(D-10)}$$

where

$$\varphi_o = \arctan\left(\frac{dy}{dx}\right)_o$$

Hence, the moment is related to Δx as follows:

$$M = 2p\rho_o\,\Delta x\sqrt{1 + \left(\frac{dy}{dx}\right)_o^2}\cos(\sigma_o - \varphi_o) \qquad \text{(D-11)}$$

The initial stiffness of the cylinder is therefore

$$\left(\frac{M}{\theta}\right)_o = \frac{p\rho_o w}{2}\,\frac{\sqrt{1 + \left(\frac{dy}{dx}\right)^2}}{\left(\frac{dy}{dx}\right)_o}\cos(\sigma_o - \varphi_o) \qquad \text{D-12)}$$

Here ρ_o and σ_o belong to the initial geometry. This expression may be

simplified by substituting $\tan\varphi_o$ for $\left(\frac{dy}{dx}\right)_o$. This gives

$$\left(\frac{M}{\theta}\right)_o = \frac{pw}{2}\left[\rho_o \cos\sigma_o \cot\varphi_o + \rho_o \sin\sigma_o\right]$$

or

$$\left(\frac{M}{\theta}\right)_o = \frac{pw^2}{4}\left[\cot\varphi_o + \tan\sigma_o\right] \qquad \text{(D-13)}$$

Since

$$\cot\varphi = \frac{dx}{dy}$$

where

$$y = \rho \sin\sigma = \frac{s}{2\sigma} \sin\sigma$$

$$x = \rho \cos\sigma = \frac{s}{2\sigma} \cos\sigma$$

it can be readily verified that

$$\cot\varphi = \frac{\cos\sigma + \sigma \sin\sigma}{\sin\sigma - \sigma \cos\sigma} \qquad \text{(D-14)}$$

This function was discussed in the compression-load section.

E. Deformation Under Combined Loads

Figure 10 shows the cross section of the cylinder as deformed under an arbitrary load having compressive, shearing, and rolling components. For the sake of convenience, a coordinate system has been chosen such that the lower plate remains fixed and the deflection of the upper plate is measured relative to the lower plate. Furthermore, the components of the load on the upper plate are taken such that they remain oriented rectangularly with the lower plate. The set of equations which describe the cross section in terms of the angles α, β, θ can be written readily in the manner used previously for the special cases:

$$\rho_1 \cos\alpha_1 = \frac{w-a}{2} - \frac{M}{pw}, \quad a = F/p \qquad \text{(E-1)}$$

$$\rho_2 \cos\alpha_2 = \frac{w-a}{2} + \frac{M}{pw} \qquad \text{(E-2)}$$

$$\rho_2 \sin\alpha_2 - \rho_1 \sin\alpha_1 = b, \quad b = \frac{Q}{p} \qquad \text{(E-3)}$$

$$\rho_1 \cos\beta_1 + \rho_2 \cos\beta_2 = w\cos\theta - a \qquad \text{(E-4)}$$

$$\rho_1 \sin\beta_1 - \rho_2 \sin\beta_2 = b - w\sin\theta \qquad \text{(E-5)}$$

Furthermore, the arc-length relation holds:

$$\left.\begin{aligned} 2\rho_1(\alpha_1 + \beta_1) &= s \\ 2\rho_2(\alpha_2 + \beta_2) &= s \end{aligned}\right\} \qquad \text{(E-6)}$$

If equations (E-6) are substituted for ρ in equations (E-1) through (E-5), the result is a set of five simultaneous equations with five unknows: α_1 α_2 β_1 β_2 θ . Solution of this set will yield the dimensions of the cross section.

An alternate method of describing the cross-section geometry is by the use of angles σ and γ :

$$\left.\begin{aligned} \sigma_1 &= \frac{\alpha_1 + \beta_1}{2}, \quad \sigma_2 = \frac{\alpha_2 + \beta_2}{2} \\ \gamma_1 &= \frac{\alpha_1 - \beta_1}{2}, \quad \gamma_2 = \frac{\alpha_2 - \beta_2}{2} \end{aligned}\right\} \qquad \text{(E-7)}$$

With this set of variables the arc-length condition is somewhat more easily applied:

$$2\rho_1\sigma_1 = 2\rho_2\sigma_2 = s \qquad \text{(E-8)}$$

The equations defining the geometry of the cross section in terms of the new variables are as follows:

$$\rho_1 \cos\sigma_1 \cos\gamma_1 + \rho_1 \sin\sigma_1 \sin\gamma_1 = \frac{w-a}{2} - \frac{M}{pw} \qquad \text{(E-9)}$$

$$\rho_2 \cos\sigma_2 \cos\gamma_2 + \rho_2 \sin\sigma_2 \sin\gamma_2 = \frac{w-a}{2} + \frac{M}{pw} \qquad \text{(E-10)}$$

$$\rho_2 \sin\sigma_2 \cos\gamma_2 - \rho_1 \sin\sigma_1 \cos\gamma_1 = \frac{w}{2}\sin\theta \qquad \text{(E-11)}$$

$$\rho_2 \sin\sigma_2 \sin\gamma_2 + \rho_1 \sin\sigma_1 \sin\gamma_1 = -\frac{w}{2}(1-\cos\theta) \qquad \text{(E-12)}$$

$$\rho_2 \cos\sigma_2 \sin\gamma_2 - \rho_1 \cos\sigma_1 \sin\gamma_1 = b - \frac{w}{2}\sin\theta \qquad \text{(E-13)}$$

Analytical solution of a set of equations such as these is not a practical matter. Numerical solutions can be obtained by iteration using a digital computer. The nature of the problem is such that the system can also be solved for any given set of the parameters quite readily by a graphical iteration method. This method is illustrated in Figure 11.

The graphical solution depends first on locating the two centers of curvature with respect to each other. This can be done at once provided the loads F and Q are known. Given the center pattern, then, it is possible to construct for each of the four corners of the cross section a locus which will include the correct position of the corner. The loci for the edges of the lower plate are necessarily vertical lines, since the distances $\rho_1 \cos\alpha_1$ and $\rho_2 \cos\alpha_2$ are fixed by equations (E-1) and (E-2), and since the distance a is by definition measured in a direction parallel to the lower plate. It should be observed that the displacement of the two centers of curvature is a direct superposition of the shifts due to each of the three components of the load, taken separately. Thus, the horizontal and vertical separations, a and b, are both proportional to and in directions perpendicular to their associated load components, and the lateral displacement of the pattern itself is proportional to the moment.

The loci for the corners of the upper plate are shown on the diagram as curves. These curves have the property that every point on them lies a fixed distance from the vertical locus (of the lower plate) along a circular arc centered on the predetermined center of curvature. Thus, regardless of the position of the lower plate, the corners of the upper plate will lie on these loci.

Once the loci are established the iterative solution may proceed rapidly using the conditions that the lower plate is horizontal and that the upper plate has width w. The partial solution indicated in Figure 11 shows the iterative path: A position is assumed for the lower plate and the corresponding position for the upper right-hand corner by swinging an arc about Center 2. The tentative position of the upper left-hand corner is found by swinging an arc of radius w from Locus 2 to Locus 1. This position is extrapolated to the lower plate with an arc about Center 1 down to the vertical locus, thereby improving the initial assumption. This process appears to have the characteristics that it converges in one direction (i. e., counterclockwise in the example) and diverges in the other.

Consider now the case of combined shear and compression for which antisymmetry is retained. In this case

$$\begin{aligned} \alpha_1 &= \beta_2 = \sigma - \gamma \\ \beta_1 &= \alpha_2 = \sigma + \gamma \\ \sigma_1 &= \sigma_2 = \sigma = \frac{\alpha+\beta}{2} \\ \gamma_2 &= -\gamma_1 = \gamma = \frac{\alpha-\beta}{2} \end{aligned} \qquad \text{(E-14)}$$

Equations (E-1) through (E-5) therefore reduce to

$$\begin{aligned} 2\rho \cos\sigma \cos\gamma &= w - a \\ 2\rho \cos\sigma \sin\gamma &= b \\ 2\rho \sin\sigma \sin\gamma &= -\frac{2M}{pw} = e \end{aligned} \qquad \text{(E-15)}$$

In addition, we can write

$$2\rho \sin\sigma \cos\gamma = h$$

Of these four relations any one can be considered redundant. Note that h and e are the height and the shear offset as used in the shear-load case.

The restoring moment M is necessary for static equilibrium. Thus

$$-2M = Qh + Fe \qquad \text{(E-16)}$$

The negative sign on the moment is necessary because of the direction of rotation of M in Figure 9.

A final reduction of the four (σ, γ) relations gives

$$\begin{aligned} \tan\sigma &= \frac{h}{w-a} = \frac{e}{b} \\ \tan\gamma &= \frac{e}{h} = \frac{b}{w-a} \end{aligned} \qquad \text{(E-18)}$$

These equations are identical to those derived for the pure shear case except that $(w-a)$ here replaces w. Thus, the shear behavior of the cylinder under a compression load is the same as that of an unloaded cylinder with the same membrane geometry. Note that the shear spring rate is

$$\frac{1}{p}\frac{dQ}{d\gamma} = \frac{w-a}{\cos^2\gamma} \qquad \text{(E-19)}$$

If $w=a$ the shear spring rate is zero, and for compression loads greater than $F=pw$ the cylinder is unstable in shear.

REFERENCES

1. Leonard, R. W., G. W. Brooks, and H. G. McComb: Structural Considerations of Inflatable Reentry Vehicles. NASA TN D-457, Sept. 1960.

2. McComb, H. G., Jr.: A Linear Theory for Inflatable Plates of Arbitrary Shape. NASA TN D-930, Oct. 1961.

3. Stroud, W. J. : Experimental and Theoretical Deflections and Natural Frequencies of an Inflatable Fabric Plate. NASA TN D-931, Oct. 1961.

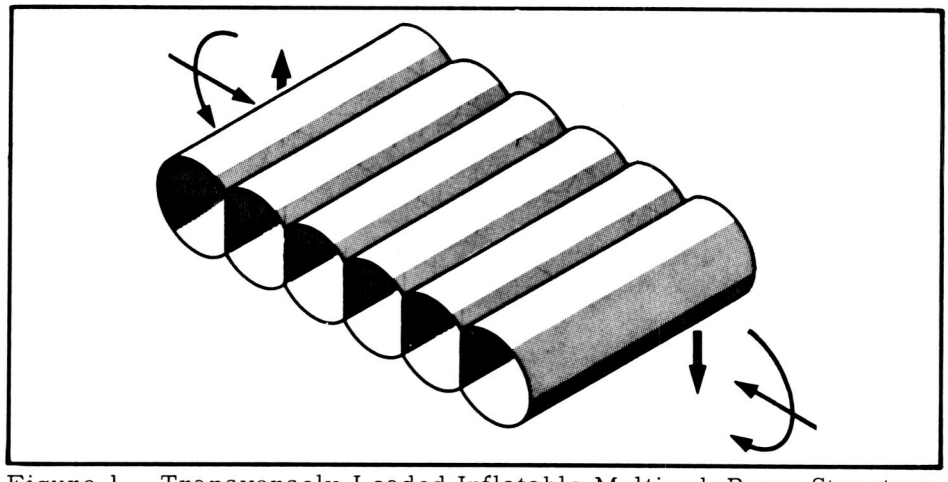

Figure 1. Transversely Loaded Inflatable Multiweb Beam Structure.

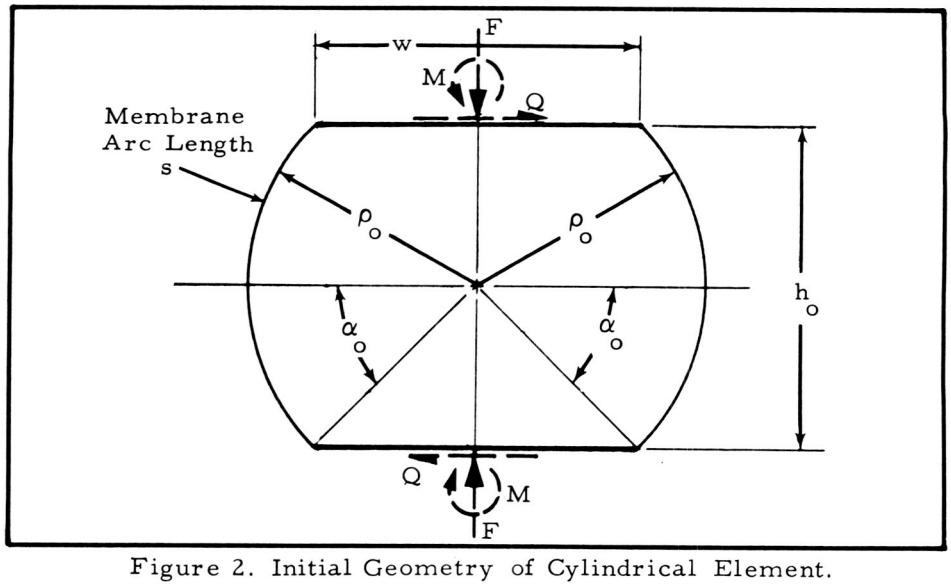

Figure 2. Initial Geometry of Cylindrical Element.

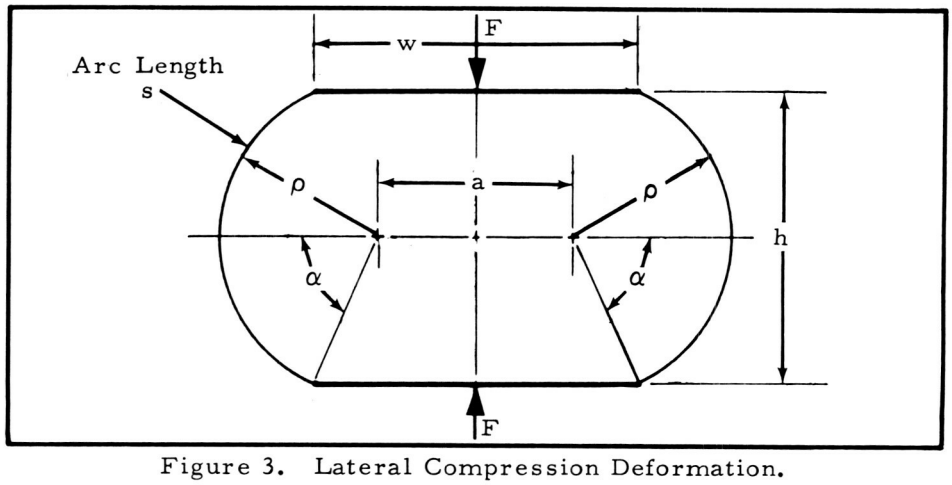

Figure 3. Lateral Compression Deformation.

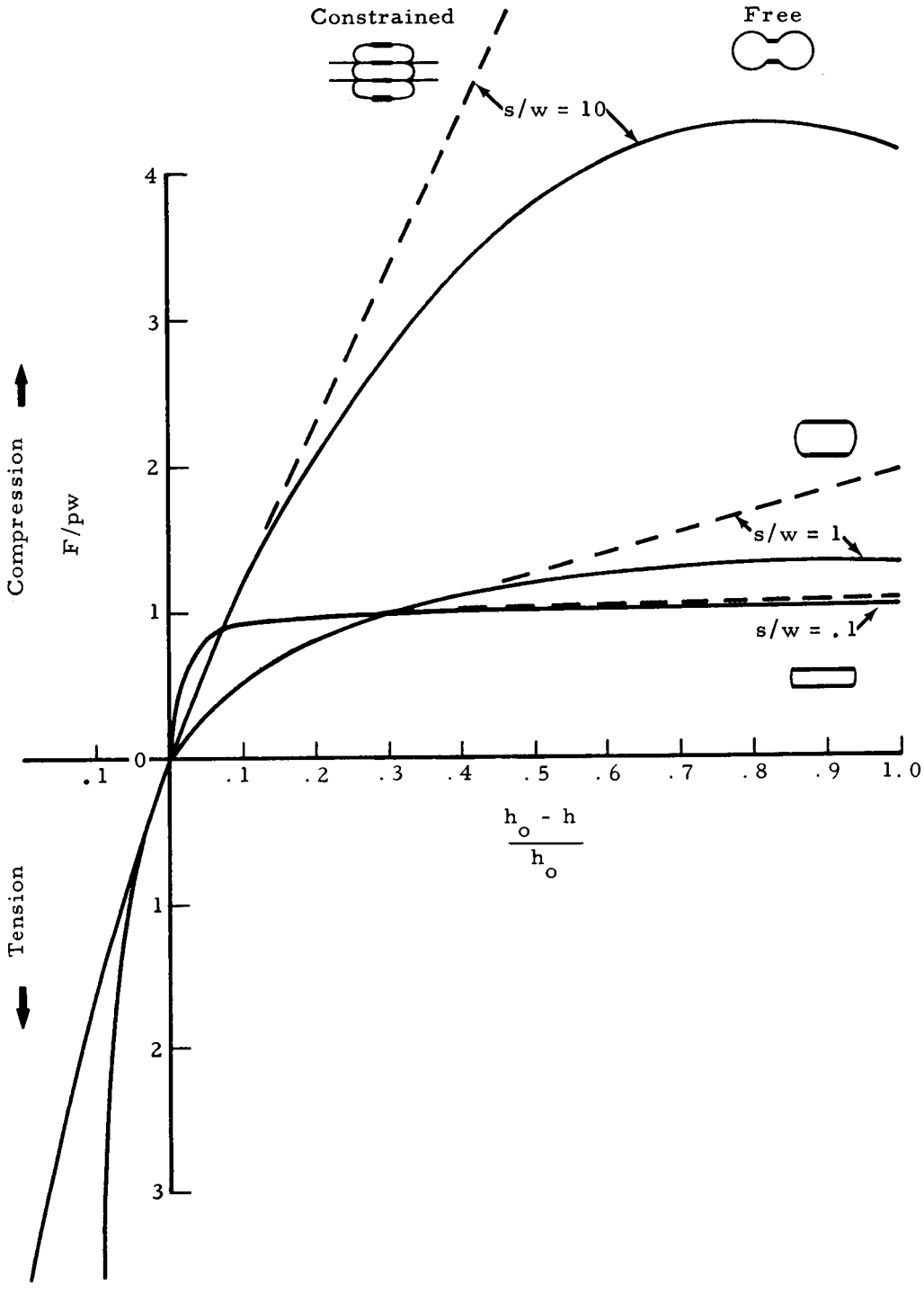

Figure 4. Compression-Load vs Deformation Characteristics.

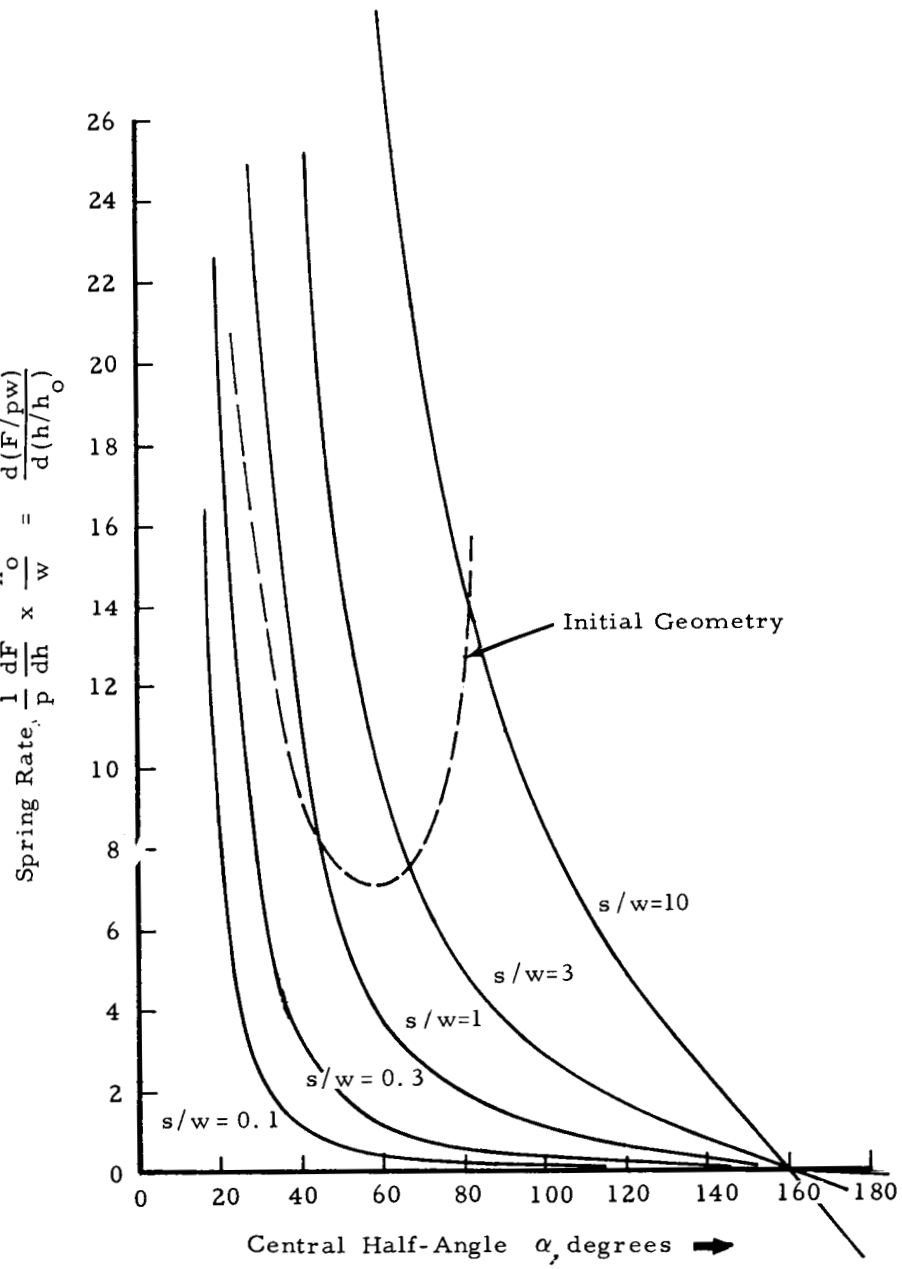

Figure 5. Compression-Load Spring Rate.

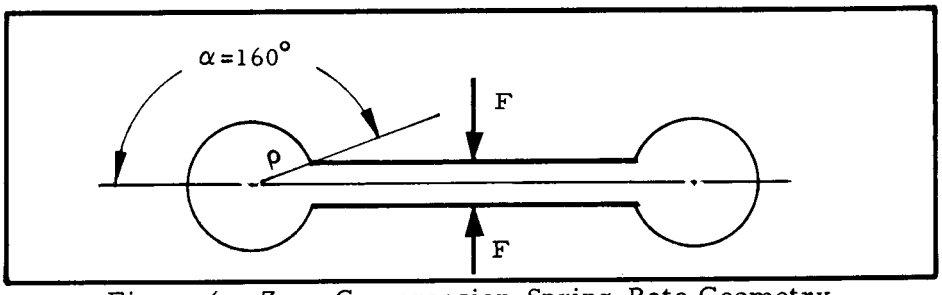

Figure 6. Zero Compression-Spring-Rate Geometry.

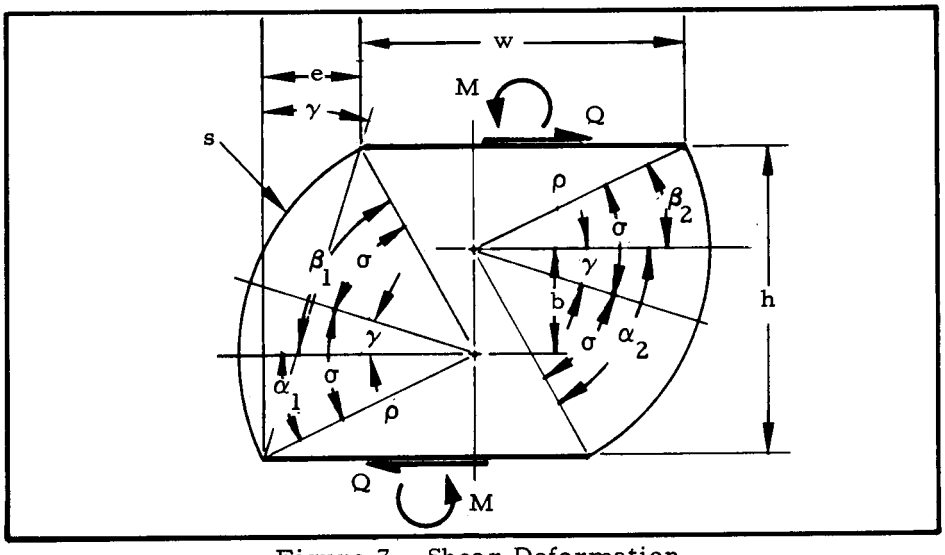

Figure 7. Shear Deformation.

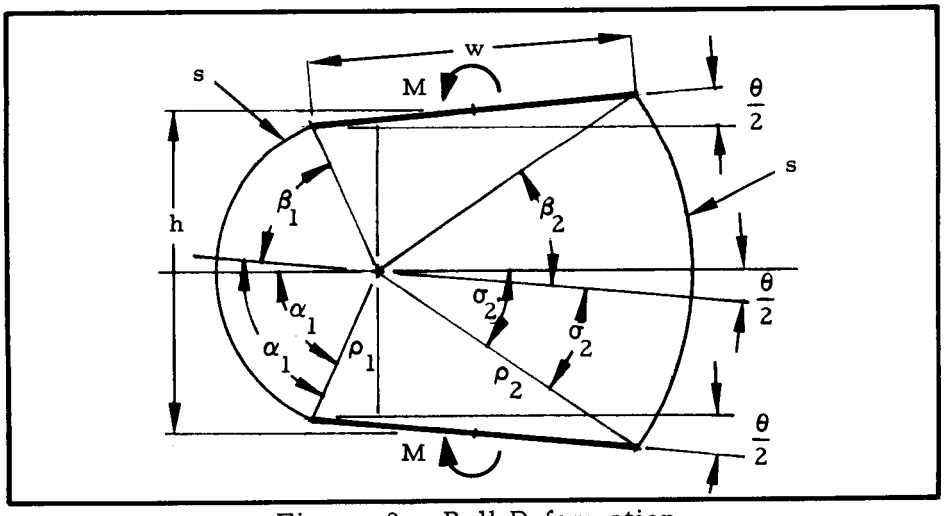

Figure 8. Roll Deformation.

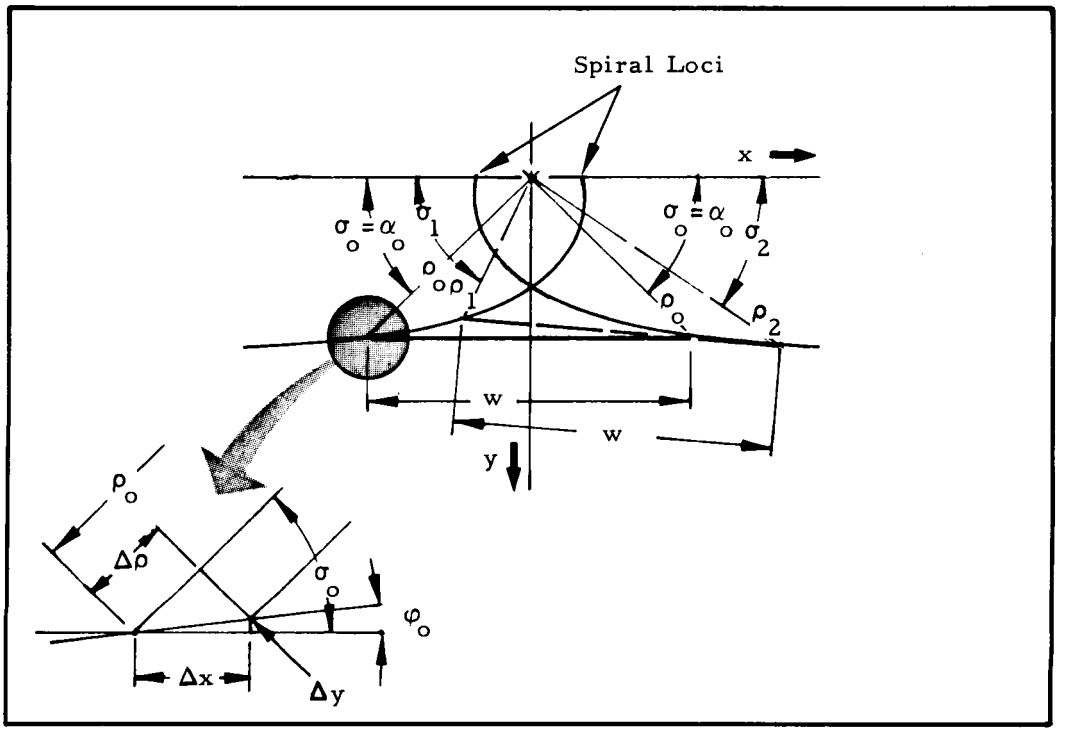

Figure 9. Graphical Solution for Roll Deformation.

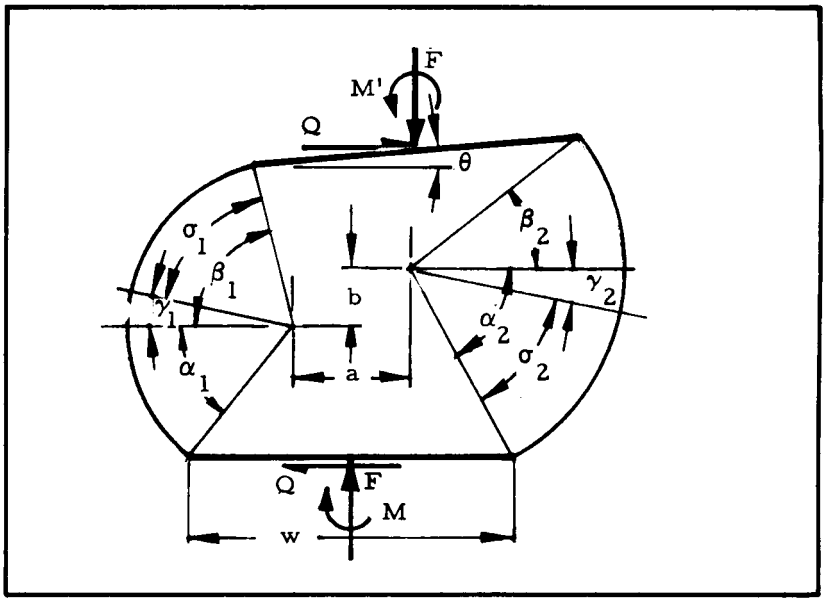

Figure 10. Combined Load Deformation.

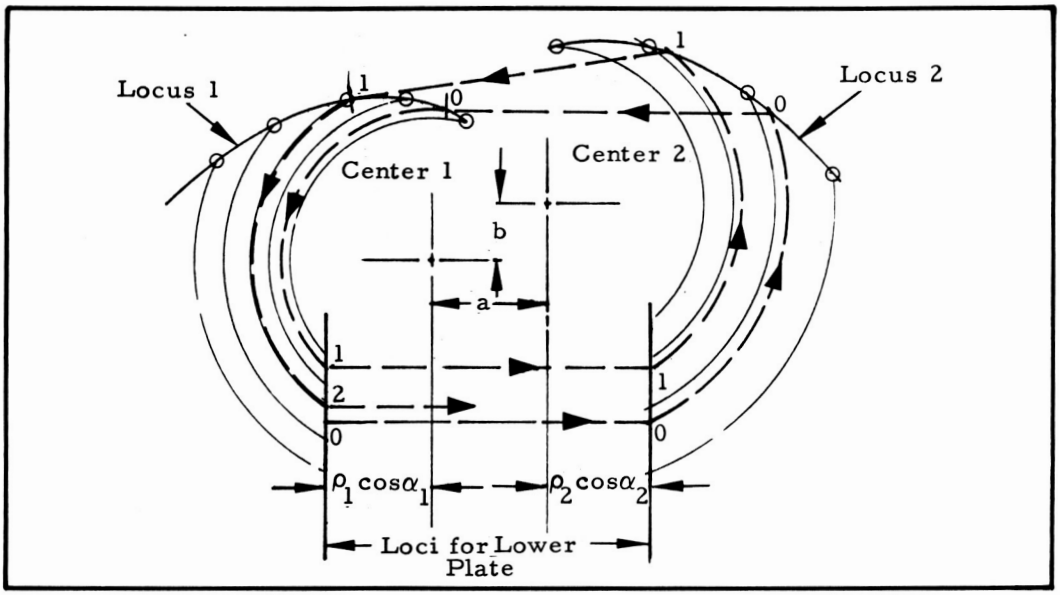

Figure 11. Graphical Solution for Combined-Load Deformation.

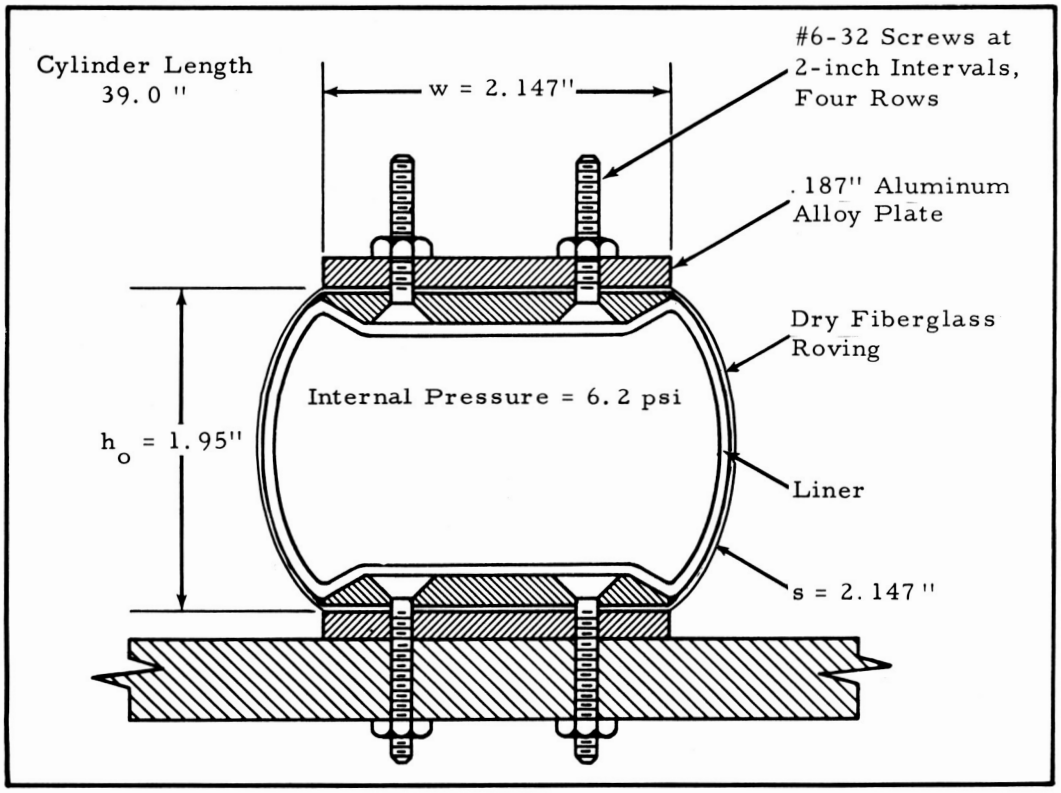

Figure 12. Diagram of Experimental Cylinder Model.

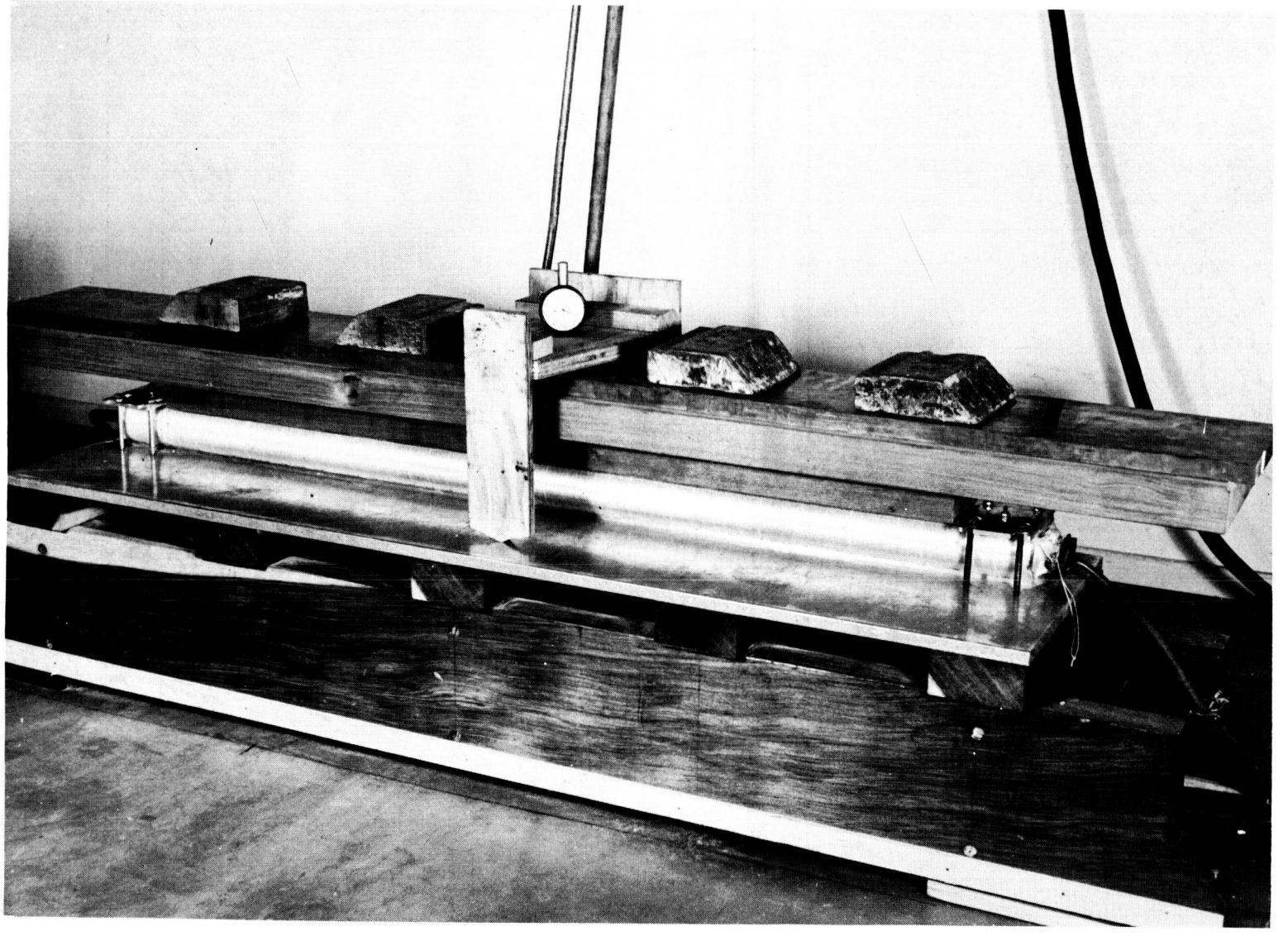

Figure 13. Experimental Cylinder Model, Compression Test.

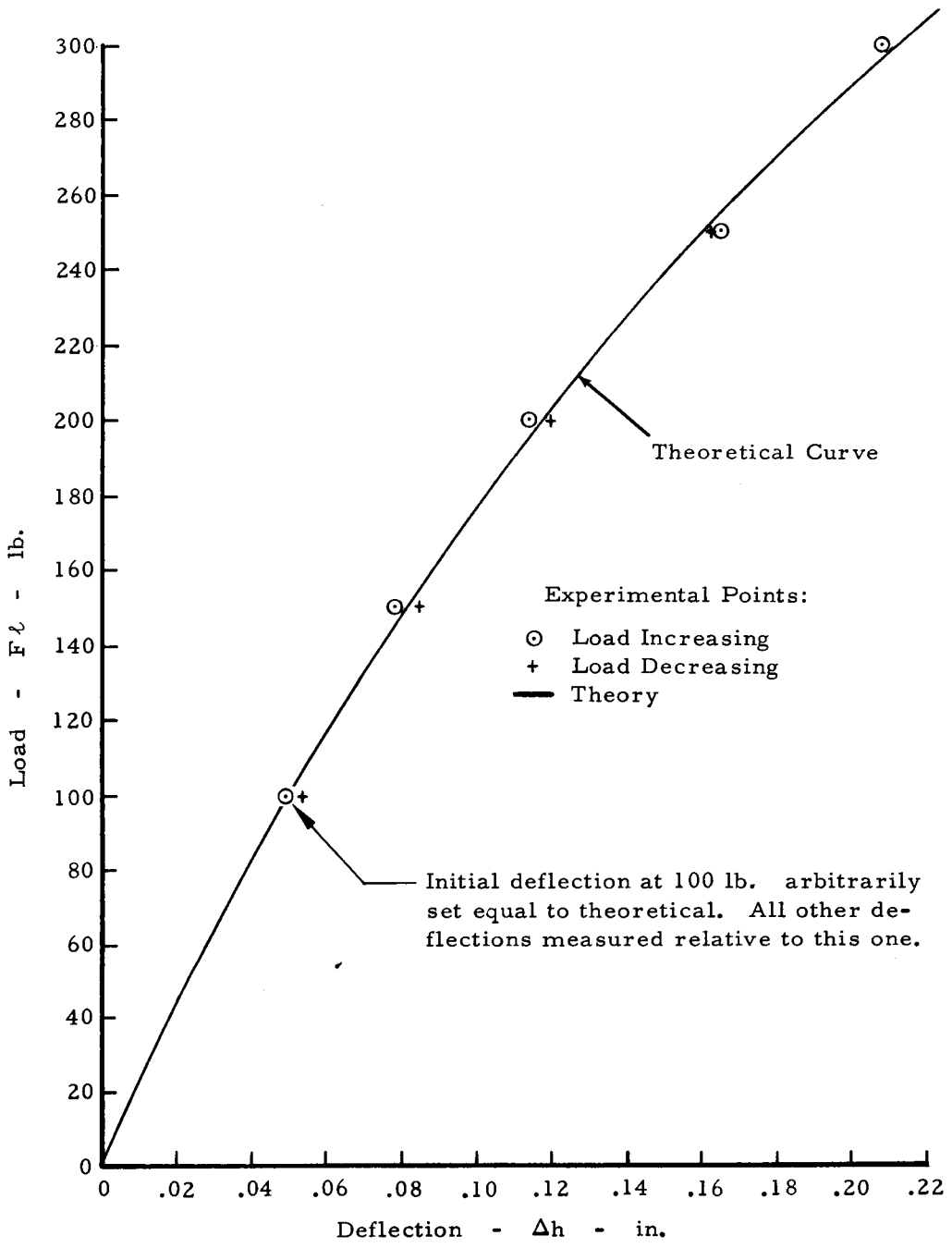

Figure 14. Compression Deformation Experiment.

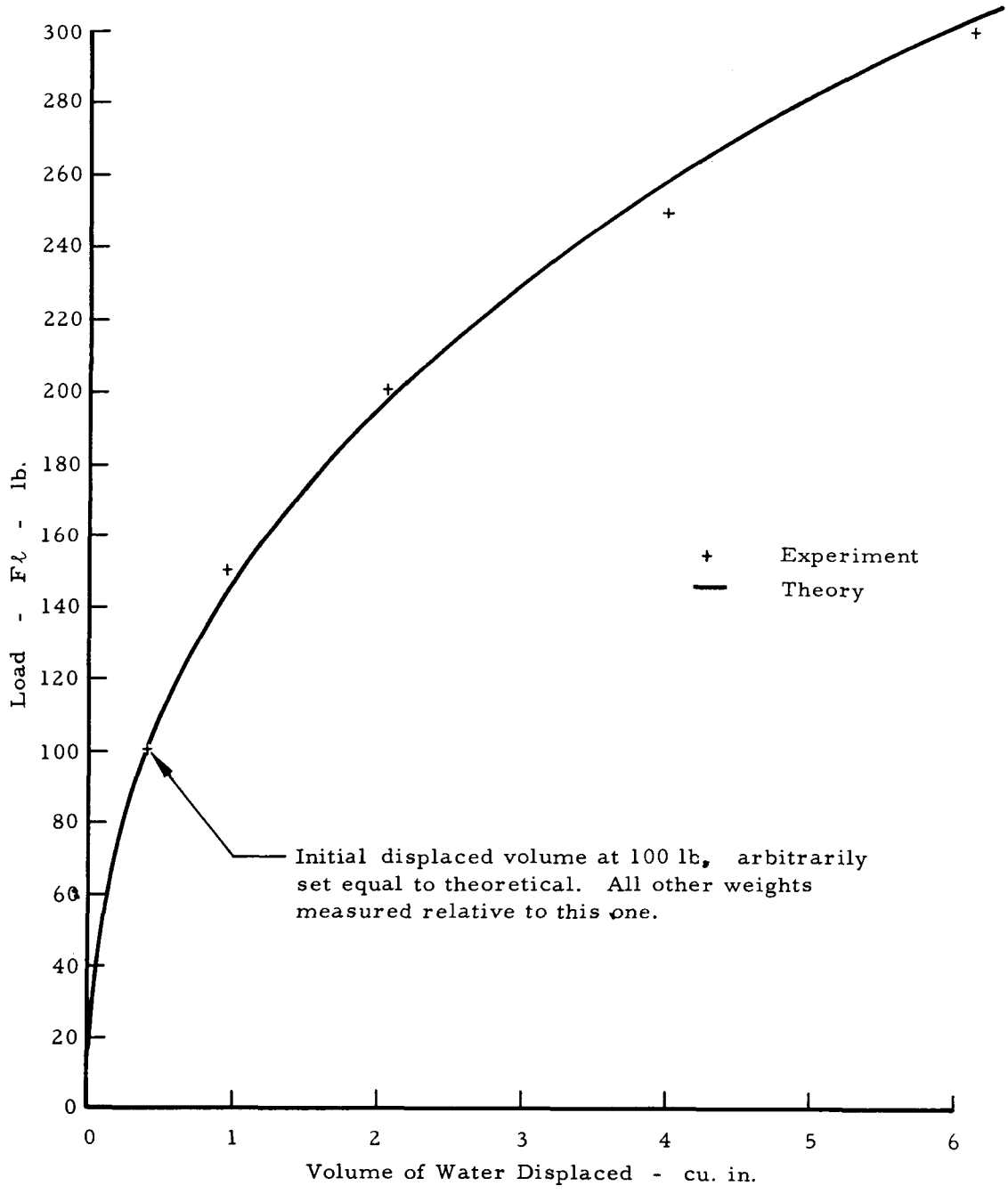

Figure 15. Compression Volume-Change Experiment.

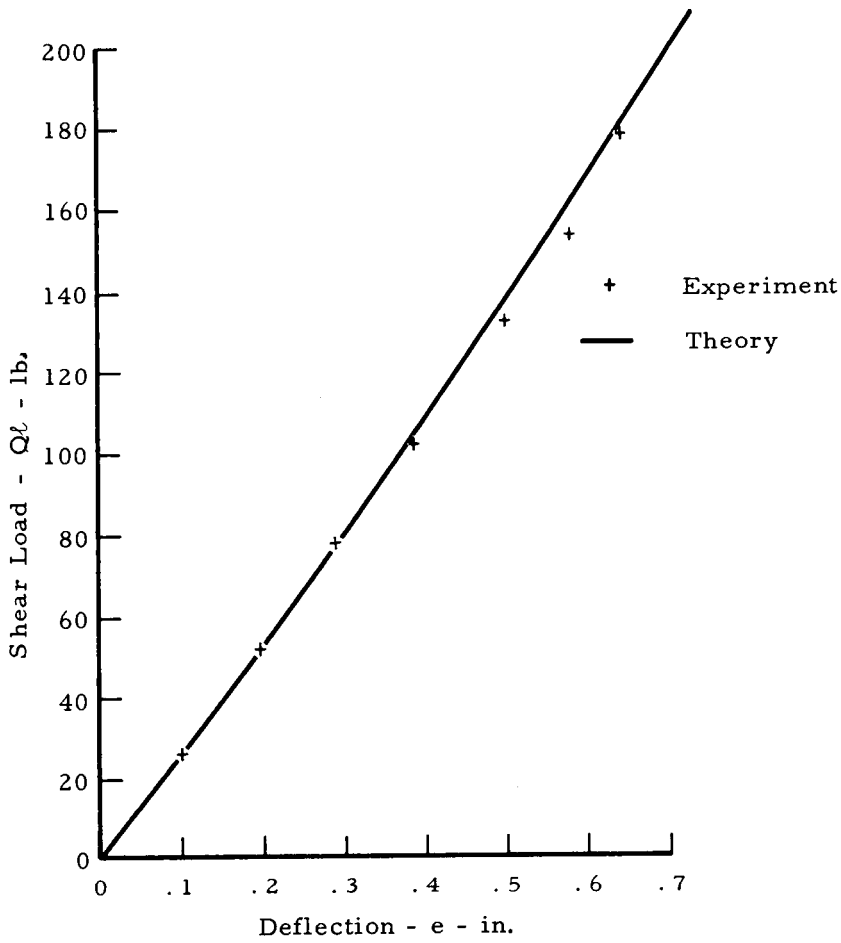

Figure 16. Shear Deformation Experiment.

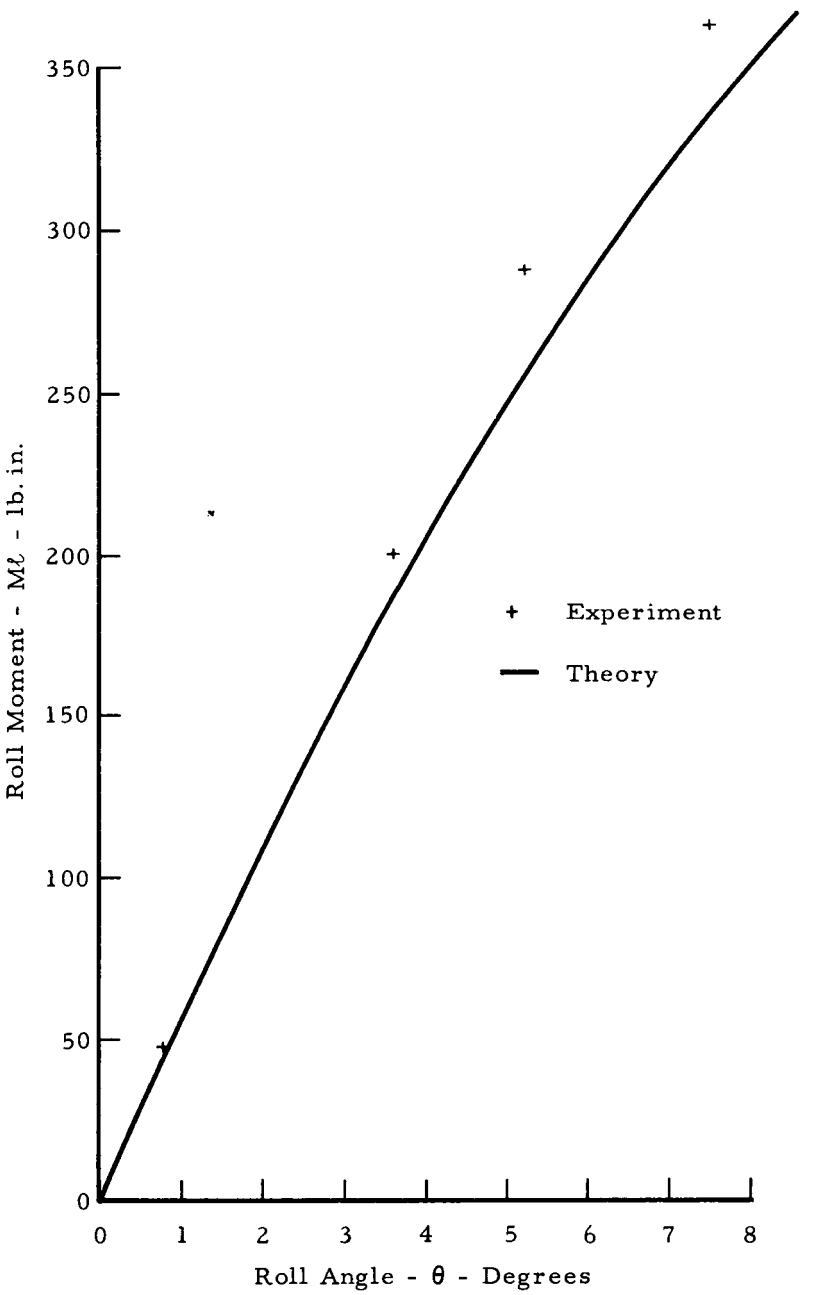

Figure 17. Roll Deformation Experiment.

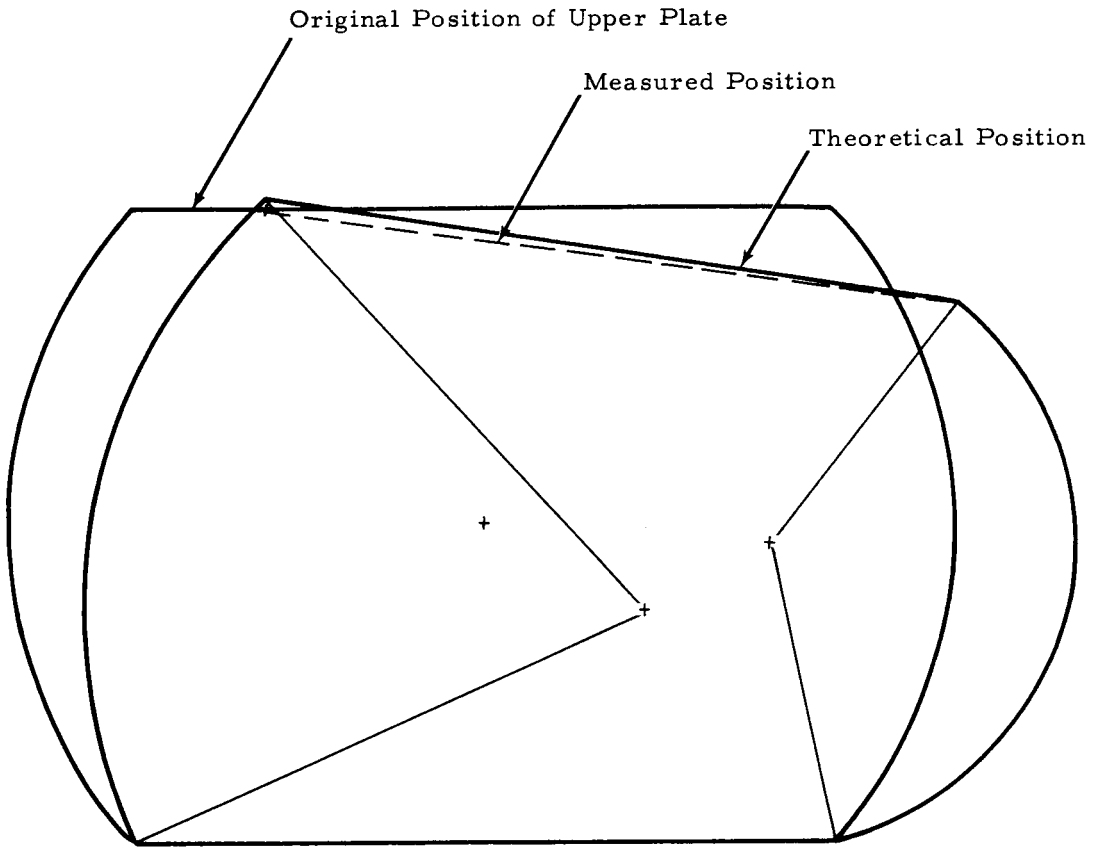

Figure 18. Combined-Load Deformation Experiment.

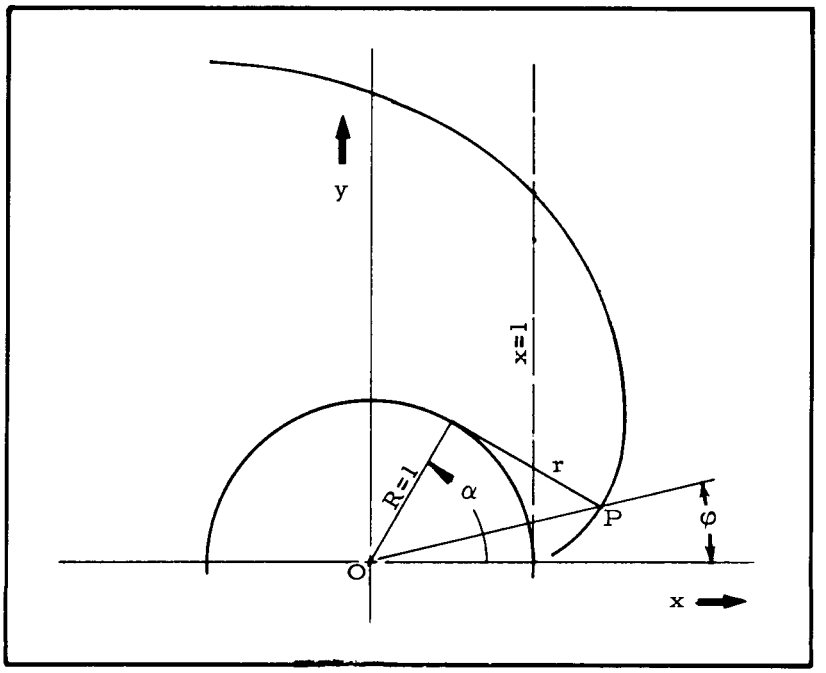

Figure 19. Involute of Unit Circle.

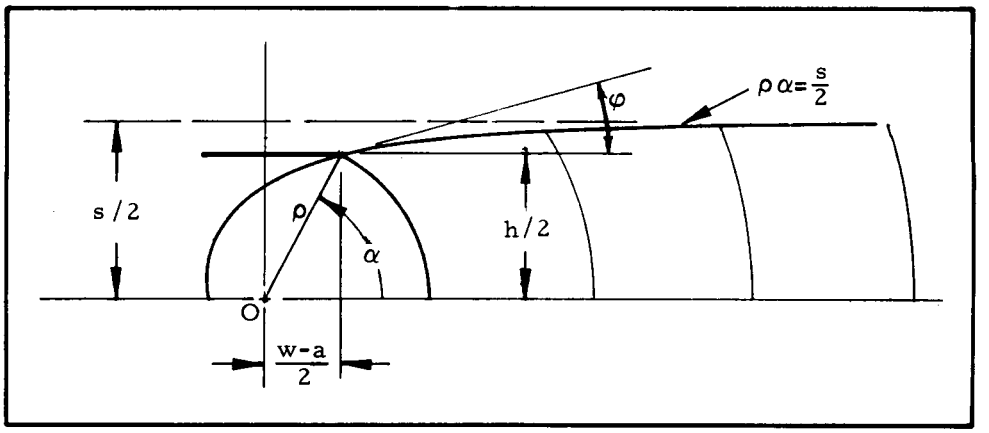

Figure 20. Hyperbolic Spiral.